Gallium Electromagnetic (GEM) Thruster Performance Measurements

IEPC-2009-233

Presented at the 31st International Electric Propulsion Conference, University of Michigan, Ann Arbor, Michigan, USA September 20–24, 2009

Robert E. Thomas* and Rodney L. Burton †
University of Illinois, Urbana, IL, 61801

Kurt A. Polzin‡
NASA-Marshall Space Flight Center, Huntsville, AL, 35812

Discharge current, terminal voltage, and mass bit measurements are performed on a coaxial gallium electromagnetic thruster at discharge currents in the range of 7-23 kA. It is found that the mass bit varies quadratically with the discharge current which yields a constant exhaust velocity of 20 km/s. Increasing the electrode radius ratio of the thruster from to 2.6 to 3.4 increases the thruster efficiency from 21% to 30%. When operating with a central gallium anode, macroparticles are ejected at all energy levels tested. A central gallium cathode ejects macroparticles when the current density exceeds 3.7 $\times 10^8$ A/m^2. A spatially and temporally broad spectroscopic survey in the 220-520 nm range is used to determine which species are present in the plasma. The spectra show that neutral, singly, and doubly ionized gallium species are present in the discharge, as well as annular electrode species at higher energy levels. Axial Langmuir triple probe measurements yield electron temperatures in the range of 0.8-3.8 eV and electron densities in the range of 8×10^{20} to 1.6×10^{21} m^{-3}. Triple probe measurements suggest an exhaust plume with a divergence angle of 9°, and a completely doubly ionized plasma at the ablating thruster cathode.

Nomenclature

A	= vapor pressure constant; area, m^2	V_{arc}	= arc voltage, V
B	= curve fit coefficient; vapor pressure constant	V_p	= plasma potential, V
I	= current, A	Z	= charge state; impedance Ω
I_{EM}	= electromagnetic impulse bit, N-s	α	= curve fit coefficient; charge parameter
k	= Boltzmann constant, J/K	β	= ablation exponent
L	= inductance, H	Γ	= particle mass flux, m^{-2} s^{-1}
m	= ion mass, kg; mass bit, kg	ϵ_o	= permittivity of free space, F/m
P	= power, W	η	= thruster efficiency
P_v	= vapor pressure, Pa	λ_D	= Debye length, m
R	= radius, m	μ_o	= vacuum permeability H/m
T	= thrust, N	χ	= non-dimensional potential
T_e	= electron temperature, K	ψ	= integral of current action, A^2-s
u_e	= exhaust velocity, m/s		

*Graduate Research Assistant, Department of Aerospace Engineering.
†Professor, Department of Aerospace Engineering.
‡Propulsion Research Scientist, Propulsion Research and Technology Applications Branch, Propulsion Systems Dept.

I. Introduction

THE gallium electromagnetic (GEM) thruster[1–3] is an electromagnetic thruster that ablates central electrode material for propellant mass. Gallium appears to offer numerous advantages over propellants currently in use. The non-toxicity and high liquid temperature range (30 °C - 2204 °C) provide numerous system advantages, while the high atomic mass and low ionization potential (5.99 eV) predict low frozen flow losses. By ablating the gallium electrode to provide discharge propellant, the electrode ablation and sheath losses inherent in MPD thrusters serve the useful function of vaporizing the propellant rather than simply introducing more heat that must be disposed of by a cooling system. In addition, mass injection is controlled by the arc, eliminating the need for pulsed gas valves.

In this paper we present voltage, current, and mass bit measurements taken at discharge current levels in the range of 7-23 kA. Emission spectroscopy measurements are undertaken to examine the atomic and ionic species present in the discharge. Axial triple probe measurements are taken to determine the electron temperature and density along the center-line of the the thruster.

I.A. Basic Scaling Relations

The thrust of self-field electromagnetic thrusters follows a quadratic dependence[4] on the discharge current

$$T = \frac{1}{2}L'I^2, \text{where } L' = 2\left[\frac{\mu_o}{4\pi}\left(\ln\frac{r_o}{r_i} + \frac{3}{4}\right)\right] \tag{1}$$

The exhaust velocity is found by dividing the thrust by the mass flow rate

$$u_e = \frac{T}{\dot{m}} \tag{2}$$

For ablative-type thrusters, it is convenient to write the mass flow rate as following a power law dependence with the discharge current

$$\dot{m} \propto I^\beta \tag{3}$$

where β is an ablation exponent. Note that for gas-fed thrusters, the mass flow rate is independent of the discharge current and $\beta = 0$. Substituting Eqns. (1) and (3) into (2), we find

$$u_e \propto I^{2-\beta} \tag{4}$$

The power across the discharge is given by

$$P = IV_{arc} \propto \frac{1}{2}\dot{m}u_e^2 \tag{5}$$

From which we find

$$V_{arc} \propto I^{3-\beta} \tag{6}$$

Therefore, by examining the V-I characteristics and mass bit as a function of current, we can obtain a general understanding of thruster performance. The performance of the Teflon PPT,[5] Teflon MPD,[6] and the graphite MPD[7] has been investigated. For all three thruster types the discharge current, arc voltage, and thrust were measured as a function of input energy. The exhaust velocity was found by dividing the impulse by the measured mass bit. In both Teflon-fed thrusters, the propellant is ablated when an arc is struck between coaxial metal electrodes. The graphite MPD is similar to the GEM thruster in that the electrode material is directly ablated as the propellant.

In order to compare the performance of ablative thrusters with varying pulse lengths and discharge current levels, the integral of the current action is introduced

$$\psi = \int_0^{\tau_p} I^2(t)\ \mathrm{d}t \tag{7}$$

The V-I characteristics and ablated mass as a function of ψ are shown in Fig. 1. Both plots yield linear results for the graphite and Teflon MPD. From both equations (3) and (6), this yields $\beta = 2$, or a constant

exhaust velocity. Indeed, it was found that the exhaust velocity was invariant with the discharge current, with values of 28 km and 14 km/s, for the graphite and Teflon MPD, respectively. The PPT has an ablation exponent value of $\beta = 1.5$, and it was found that the exhaust velocity increased with discharge current.[5]

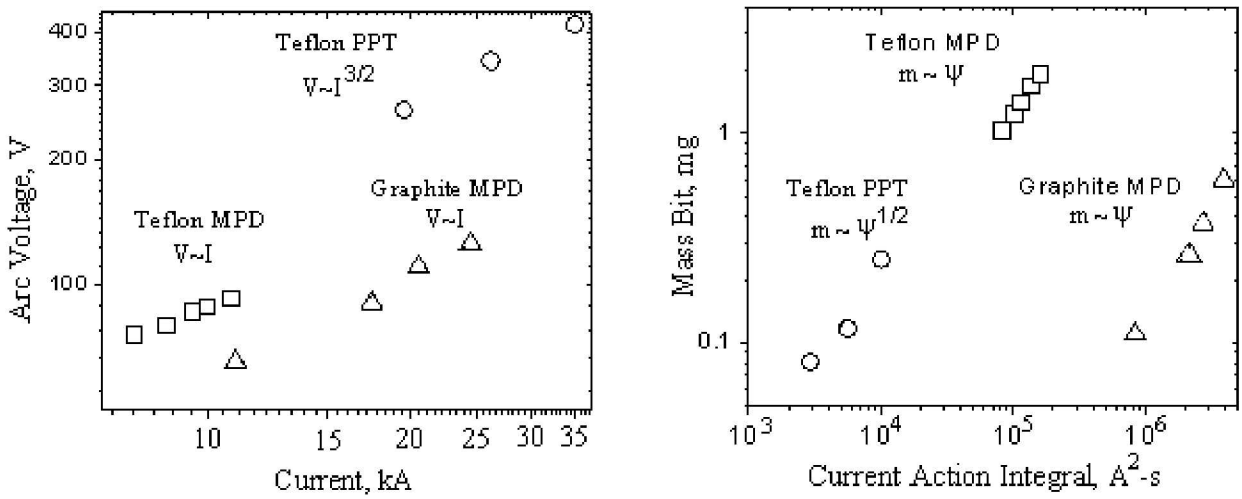

Figure 1. Voltage-current and mass bit vs. ψ plots for previously developed ablative electromagnetic thrusters. The ablation exponent is $\beta = 1$ for both the graphite and Teflon MPD, while for the Teflon PPT $\beta = 1.5$.

II. Experimental Apparatus

II.A. Testing Facilities

Tests were conducted at the University of Illinois Electric Propulsion Laboratory on the coaxial GEM thruster shown in Fig. 2. The stainless steel annular electrode has outer and inner diameters of 57.2 mm and 22.6 mm, respectively. A 8.7 mm diameter hole drilled through the center of the boron nitride insulator allows the gallium to make electrical contact with a brass standoff, which in turn is connected to a high-current pulse forming network described below. The thruster was mounted into a 5-way vacuum cross, which is attached to the main vacuum chamber. A baffle was inserted into the 5-way cross to condense and capture ejected gallium particles before they reach the main chamber. Vacuum was maintained by a TPH1500 turbomolecular pump, which is backed by two Roots blowers and two Kinney mechanical displacement pumps. The base pressure of the facility during testing was 5×10^{-5} torr.

Figure 2. Coaxial GEM thruster electrodes, and boron nitride insulator.

A ten-section, 5-line pulse forming network (PFN) was used to power the thruster. Each of the 5 sections consists of ten 88 μF capacitors in series with 85 nH inductors. The 50 capacitors have a maximum charging voltage of 1.2 kV, which yields a bank energy of 3.2 kJ. A copper sheet with punched holes was located over

the capacitors to provide a common ground (ground plane). Brass standoffs with a height of 3.8 cm were machined to provide spacing between the stage inductors and the ground plane. Two 9 cm long, 0.32 cm (1/8) diameter copper rods yield a section inductance of 85 nH. The five PFN lines were each connected in parallel using 2.5 cm wide copper strip. To minimize stray inductance in the charging circuit, the PFN was mounted close to vacuum chamber, as shown in Fig. 3. A 7.0 cm wide strip of copper sheet formed the transmission line to the thruster. The capacitors were charged using a Hipotronics DC power supply.

Figure 3. 3.2 kJ Pulse Forming Network and 1.5 m^3 vacuum tank.

III. Experimental Results

III.A. Voltage and Current Measurement

Measurements were obtained for capacitor charging voltages in the range of V_o = 150-350 V. A Pearson 4418 current monitor and Tektronix P6015A voltage probe were used to measure the discharge current and terminal voltage, respectively. Representative traces are in Fig. 4. Note that the PFN impedance is well-matched to the arc impedance, minimizing current reversal.

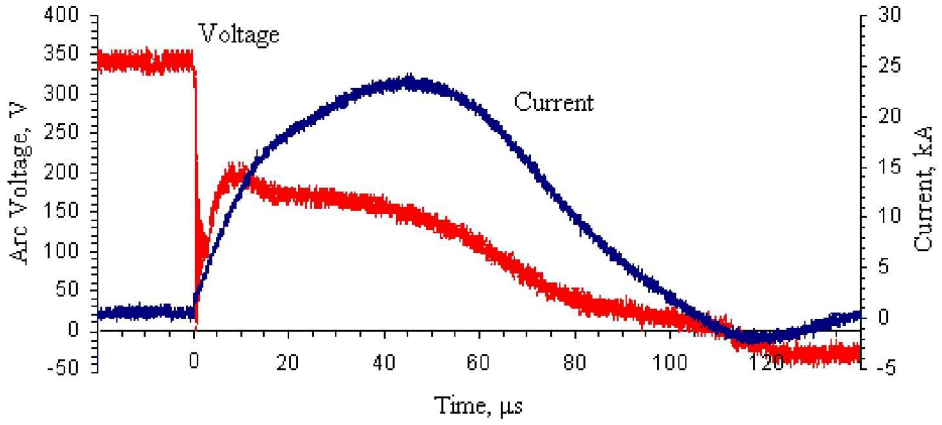

Figure 4. Representative voltage and current traces taken at 290 J.

A plot of the arc voltage vs. the discharge current is shown in Fig. 5 for an anode and cathode radius of 15 and 4.35 mm, respectively. The voltage and current data is taken at τ = 50 μs. The arc impedance varied from 6-7 mΩ, decreasing slightly with energy level. The arc voltage varies linearly with the current, resulting in an ablation exponent of $\beta = 2$.

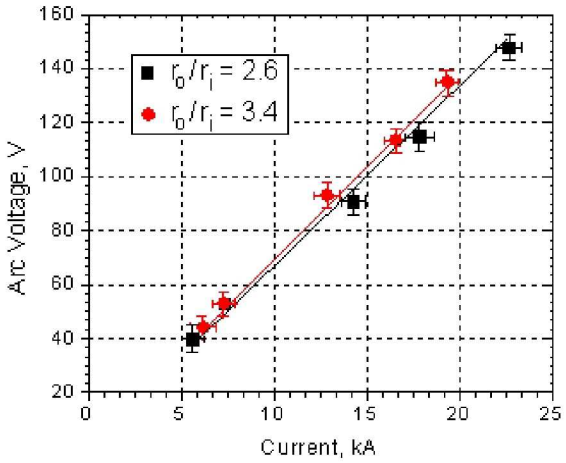

Figure 5. Plot of arc voltage as a function of discharge current.

III.B. Mass Bit Measurement

The mass ablated per pulse was measured by weighing the inner and annular electrode after a prescribed number of shots using a Mettler AG245 measurement scale with a resolution of 0.1 mg. Several hundred shots were fired which liberated at least 10 mg, leaving the error due to instrumentation at less than 1%. Tests were repeated 4 times at each energy level, and the ablated mass measurements were found to be repeatable. No visible oxidation was seen on the gallium surface before or after testing. The mass of the annular stainless steel electrode decreased slightly after each test run. However, the total amount of mass lost (i.e. 0.3 mg after 250 shots) was small compared to the total mass of ablated gallium.

Measurements were initially obtained using a 5 mm central gallium anode. It was found that in this configuration gallium sputtered from the central electrode leaving macroparticles on the insulator and outer electrode (Fig. 6). Macroparticle ejection can be eliminated by reducing the current density. This was first attempted by lowering the discharge current, and when this failed, by increasing the diameter of the gallium electrode from 5, 7.1 and then 8.7 mm. This proved unsuccessful, so the polarity of the thruster was then reversed, and the measured mass bit dropped by an order of magnitude and no sputtered gallium particles were observed when using the 8.7 mm diameter gallium cathode. However, when the current exceeded roughly 22 kA (j = 3.7 $\times 10^8$ A/m^2), gallium once again sputtered from the central electrode. This set the upper limit of testing at a capacitor charging voltage of $V_o = 350$ V (290 J). The mass bit vs. ψ is shown in Fig. 7. The linearity of the plot is consistent with the V-I plot and also yields a mass ablation coefficient of $\beta = 2$.

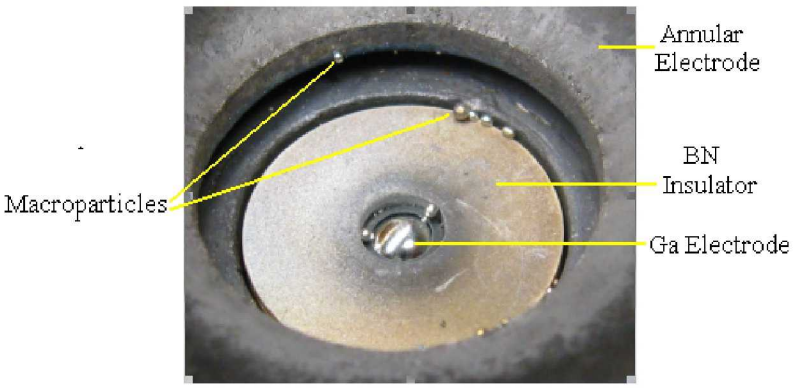

Figure 6. Macroparticles sputter onto the insulator and annular electrode when utilizing a central gallium anode.

The exhaust velocity can be estimated through use of the electromagnetic impulse bit

$$I_{EM} = \int T \, \mathrm{d}t = \frac{1}{2} L' \psi \tag{8}$$

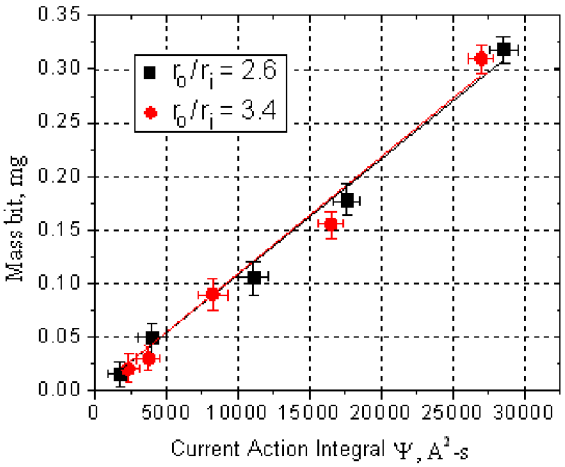

Figure 7. Measured mass bit vs. ψ parameter.

The exhaust velocity is found by dividing the impulse bit by the mass bit, m

$$u_e = \frac{I_{EM}}{m} = \frac{1}{2}\frac{L'\psi}{m} \tag{9}$$

The slope in Fig. 7 is proportional to exhaust velocity, which has values of 17 and 20 km/s for radius ratios of 2.6 and 3.4, respectively.

III.C. Langmuir Triple Probe Measurements

III.C.1. Probe Construction

The triple Langmuir probe[8] has been used successfully used to measure the electron temperature and density in MPD thrusters.[9–11] The triple probe (shown schematically in Fig. 8) consists of three separate electrodes configured such that the electron temperature and density can be reduced from the measured currents I_2 and current I_3.

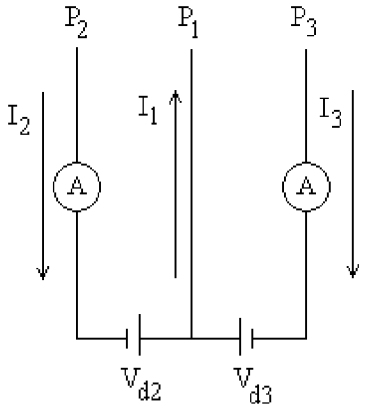

Figure 8. Triple Langmuir probe circuit.

The triple probe used in this study consisted of three 0.381 mm (0.015″) diameter tungsten wires fed through a four -bore alumina tube with an O.D. of 4.7 mm. The exposed wire length was 4.5 mm yielding a probe surface area of 5.5 ± 0.2 mm^2. The tungsten wires are connected to RG58 coaxial cables which are fed to the oscilloscope located in a shielded screen room. The applied voltages of V_{d2}= 5 V and V_{d3} = 10 V were supplied using a DC power supply floated through use of an isolation transformer.

III.C.2. Probe Theory

Use of a triple probe assumes (a) a Maxwellian electron energy distribution, (b) a thin ($r_p >> \lambda_D$) , collisionless ($\lambda_{ie}, \lambda_{ii} >> \lambda_D$) ion sheath, and (c) an ion sheath thickness smaller than the separation between probes ($d_s >> \lambda_D$). The ion sheath is on the order of the Debye length, λ_D, which is given for a quasi-neutral plasma by

$$\lambda_D = \left(\frac{\epsilon_o k T_e}{n_e e^2} \right)^{1/2} \tag{10}$$

Assuming $T_e = 2$ eV and $n_e = 10^{21}$ m^{-3}, yields a Debye length of 0.3 microns. Therefore $1 >> r_p/\lambda_D$ and the thin sheath requirement is met. The ratio of the ion-ion and ion-electron mean free paths to the Debye length are 150 and 24000, so the sheath can be assumed to be collision-less. The separation of the probes is approximately 0.5 mm, which is much greater than the Debye length.

The current flowing into the probes may be written as

$$I_1 = A J_e \exp(-\chi_1) - A J_i (B + \chi_1)^\alpha \tag{11}$$

$$I_2 = A J_e \exp(-\chi_2) - A J_i (B + \chi_2)^\alpha \tag{12}$$

$$I_3 = A J_e \exp(-\chi_3) - A J_i (B + \chi_3)^\alpha \tag{13}$$

where the dimensionless potential χ for each probe is given in terms of the plasma potential V_p.

$$\chi = \frac{e|V - V_p|}{k T_e} \tag{14}$$

The electron and ion saturation current current densities are given by

$$J_e = n_e e \left(\frac{k T_e}{2\pi m_e} \right)^{1/2} \tag{15}$$

$$J_i = n_i e \left(\frac{k T_e}{2\pi m_i} \right)^{1/2} \tag{16}$$

The coefficients α and B are found through use of the Peterson/ Talbot curve[12]

$$\alpha = \frac{2.9}{\ln(r_p/\lambda_D) + 2.3} + 0.07 \left(\frac{T_i}{Z_i T_e} \right)^{3/4} - 0.34 \tag{17}$$

$$B = 1.5 + \left(\frac{T_i}{Z_i T_e} \right) \left[0.85 + 0.135 \left(\ln \left(\frac{r_p}{\lambda_D} \right) \right)^3 \right] \tag{18}$$

Equations (10)-(18) result in a non-linear system of equations that yield T_e, n_e, and V_p.

III.C.3. Triple Probe Results

Measurements were taken on the center line of the thruster downstream of the cathode tip, at 2, 6, 12, and 18 cm. All measurements were taken at a discharge current of 23 kA. Measurements were averaged over several shots and the probes were manually cleaned in between experiments. The measured currents I_2 and current I_3 are shown in Fig. 9 for applied voltages of $V_{d2} = 5V$ and $V_{d3} = 10V$. The applied voltages where measured during each pulse and found to vary by less than 10% of the nominal value during the steady portion of the pulse.

The axial variation of the peak electron temperature and density are shown in Figs. 10 and 11, with values at an axial location 2 cm downstream of the inner electrode of 3.8 eV and 1.6 $\times 10^{21}$ m^{-3}. The sources of experimental error include: uncertainties in probe surface area and probe end effects (10%), probe misalignment (5 %), the presence of doubly ionized species (20%). The error for the electron temperature is thus estimated to be 15% with a 35% error on the number density.

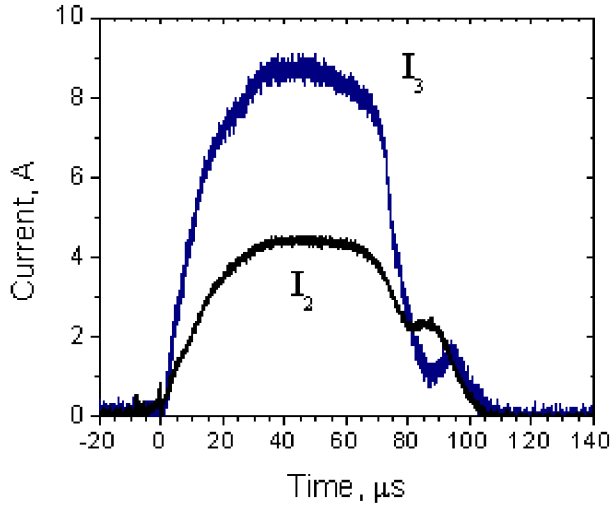

Figure 9. Collected triple probe currents taken 2 cm from cathode tip.

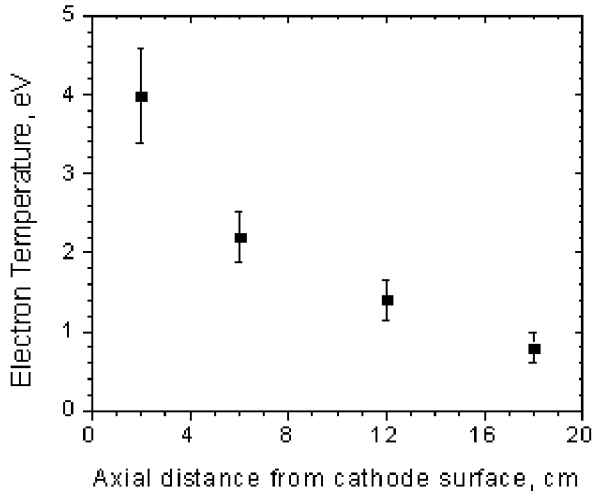

Figure 10. Center line electron temperature at four axial probe positions.

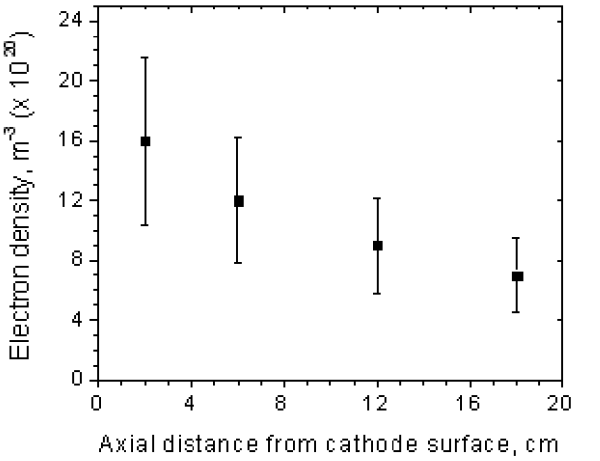

Figure 11. Center line electron density at four axial probe positions.

Extrapolating the temperature data to the face of the cathode (z = 0 cm) and assuming an expansion ratio of 100 yields an electron temperature of 5 eV and an electron density of 10^{23} m^{-3}. At this temperature and density range, the plasma is completely doubly ionized. This results in a Larmor radius of 15 mm, which is approximately the radius of the annular electrode This is suggests that the bulk of the ions will be able to drift out of the discharge region without being lost to the outer electrode. An estimate of the plume divergence can be made by assuming that the product of the particle density, exhaust velocity, and plume area is a constant ($n_e u_e A$ = const). The diameter of the expansion fan is taken to be 5 cm at a downstream distance from the cathode surface of two centimeters (Fig. 12). This yields a divergence angle of $\tan^{-1}(2.5/16) = 9°$.

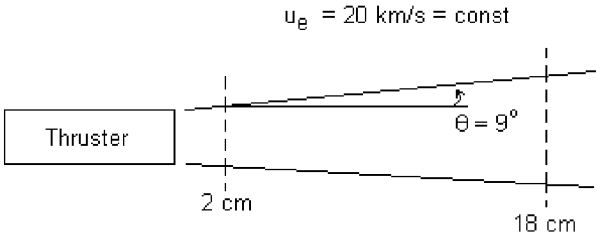

Figure 12. Plume divergence for GEM thruster.

III.D. Emission Spectroscopy

We acquired spectroscopic data from the discharge to determine which species were present. These spectra were obtained using a 25 mm focal length spectrometer with 5 micron inlet slit, yielding 0.7 nm resolution over the range of 220 nm to 520 nm. Emission was collected using a 12 mm diameter f/2 quartz plano convex lens which was focused onto the end of a 400 micron diameter silica fiber. The spectrum was time-integrated over several discharge pulses and spatially integrated over a broad region. The output of the spectrometer was wavelength-calibrated using a mercury lamp and corrected for relative spectral efficiency using a deuterium lamp.

The emission spectra were obtained at energy levels ranging from 85-290 J. Emission from neutral, singly, and doubly ionized Ga species were observed in the discharge. Iron, removed from the outer electrode, was also seen in the spectra obtained. Spectra from the 85 and 290 J cases are shown in Figs. 13 and 14. They are largely similar, however the 290 J case exhibits several iron lines as well as additional Ga III lines. A full listing of the observed gallium species is presented in the Appendix.

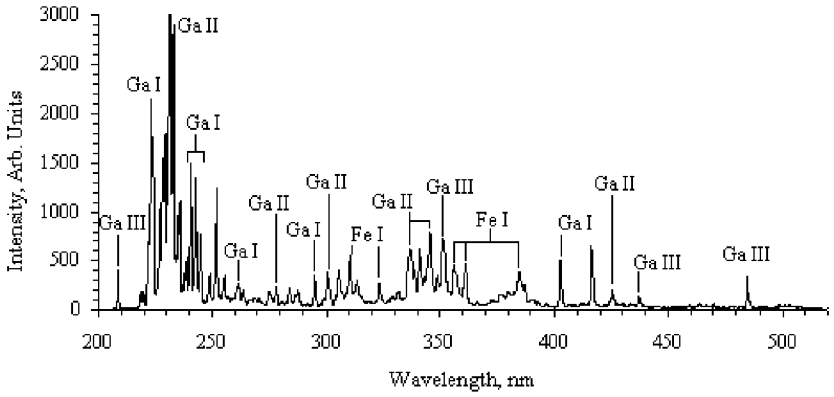

Figure 13. Emission spectra taken at energy level of 85 J.

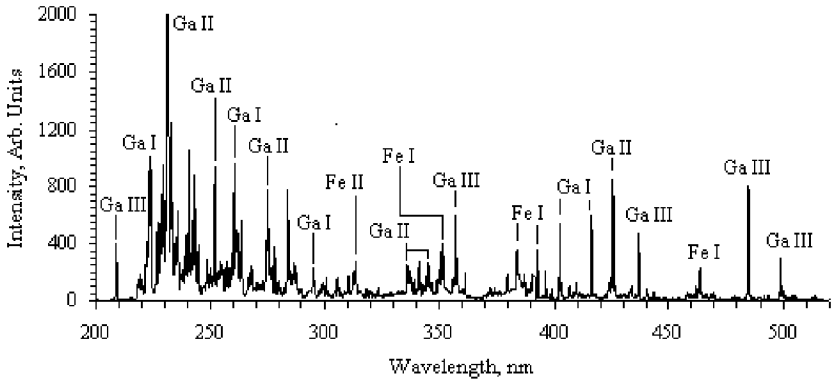

Figure 14. Emission spectra taken at energy level of 290 J.

IV. Analysis

IV.A. Efficiency Calculation

The efficiency of electric thrusters is defined as the ratio of the jet kinetic power to the input power

$$\eta = \frac{\dot{m}u_e^2}{2P_{in}} \tag{19}$$

An alternative form can be obtained by utilizing the dynamic impedance

$$Z_{dyn} = \frac{1}{4}L'u_e \tag{20}$$

and by substituting $P = IV_{arc}$ in equation 19. One obtains

$$\eta = \frac{Z_{dyn}}{Z_{arc}} = \frac{(L')^2\psi}{8mZ_{arc}} \tag{21}$$

where $Z_{arc} = Z_{dyn} + Z_{ohmic}$. An estimate of the thruster efficiency can be made from the discharge current, arc voltage, and mass bit. Tests were initially conducted on a thruster possessing a radius ratio of 2.6, which yielded a computed efficiency of 21%. Increasing the diameter of the annular electrode resulted in an increase in the efficiency to 30%. Assuming the electrical characteristics and mass bit are roughly constant for a given discharge energy, the efficiency rises to 40% at a radius ratio of 5 (Fig. 15) with an exhaust velocity of 23 km/s.

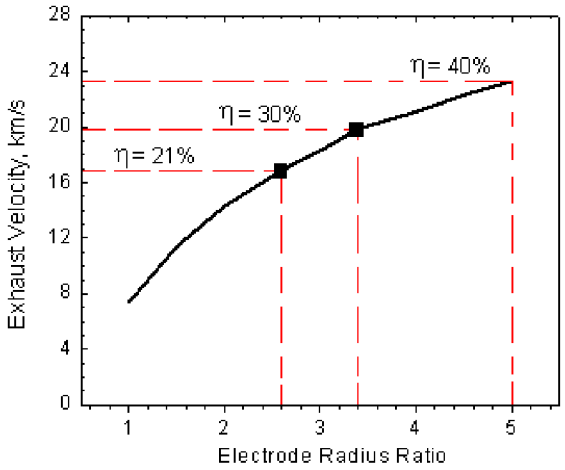

Figure 15. Exhaust velocity and thruster efficiency as a function of electrode radius ratio.

IV.B. Scaling Relations

A review of MPD performance has been presented in Ref. [2]. Two parameters of particular interest are the ion Larmor radius R_L, and the charge carrier parameter α, which represents the fraction of the discharge current that can be carried by the number of ions present

$$\alpha = \frac{Ze}{mI}\frac{dm}{dt} \tag{22}$$

An equivalent Larmor radius can be defined as:

$$R_L = 2\pi R \frac{m}{Zeu_e\mu_o I} \tag{23}$$

where μ_o is the magnetic permeability of free space and R is the average radius of the coaxial thruster. The Larmor radius and charge carrier parameter are tabulated for different propellants. It is assumed that both the ions and electrons carry the current, so the charge carrier parameter is multiplied by 2 in the Table IV.B. Additionally, for both ablative thrusters (the GEM and Carbon MPD) the charge state is taken to be $Z = 2$.

Table 1. MPD Thruster performance for various propellants

Propellant	At. Wt.	Current, kA	dm/dt, gm/s	Isp, s	Eff.	Charge Parameter, α	Larmor Rad., cm
Hydrogen	1	20	0.5	16000	0.52	4.8	1.3
Carbon	12	24	0.6	2780	0.07	0.7	0.4
Nitrogen	18	18	4.0	4000	0.37	3.2	5.0
Argon	40	20	6.0	2800	0.20	1.4	8.8
Gallium	**70**	**23**	**4.4**	**2000**	**0.30**	**1.4**	**1.5**
Xenon	131	20	6.0	1400	0.10	0.4	14.4

The results from Table IV.B suggest that efficient operation is reached when $\alpha > 1$ and the Larmor radius is smaller than the thruster channel. The efficiency tabulated for the GEM thruster (30%) corresponds to an electrode ratio of 3.4. As noted earlier, increasing the electrode ratio to 5 would yield an efficiency of 40%, which compares favorably to the thrusters shown.

IV.C. Mass Flow Rate Prediction

As noted previously the mass scales quadratically with the discharge current. An expression for the mass flow rate as a function of current can be found as follows. An estimate of the evaporation rate can be made by using the Langmuir equation, which expresses the flux of atoms released from a surface in equilibrium in terms of the surface temperature and vapor pressure[13]

$$\Gamma = \frac{P_v}{\sqrt{2\pi m k T_s}} \tag{24}$$

The vapor pressure P_v (in Pa) and surface temperature T_s (in K) are related by the Clausius-Clapeyron relation

$$\log(P_v) = 5.006 + A - \frac{B}{T_s} \tag{25}$$

where the constants have values of $A = 5.52$ and $B = 13798$, respectively for gallium.[14] The pressure due to the pinch effect is given by

$$P_{avg} = \frac{2}{3}\frac{\mu_o I^2}{8\pi^2 r_c^2} \tag{26}$$

where the factor of 2/3 has been added to account for the parabolic distribution of pressure over the cathode surface (Fig. 16). Setting the vapor pressure equal to the average pinch pressure ($P_v = P_{avg}$) yields an expression for the mass flow rate in terms of the discharge current. A comparison of the calculated vs.

experimental mass flow rate is shown in Fig. 17. It can be seen that the mass flow rate predicted using the pinch model is consistently higher than the measured value. This may be due to a lower than expected liquid gallium surface temperature, due to heat conduction into the liquid. An additional effect is a non-uniform current density, which could reduced the 2/3 factor and also the ablated mass.

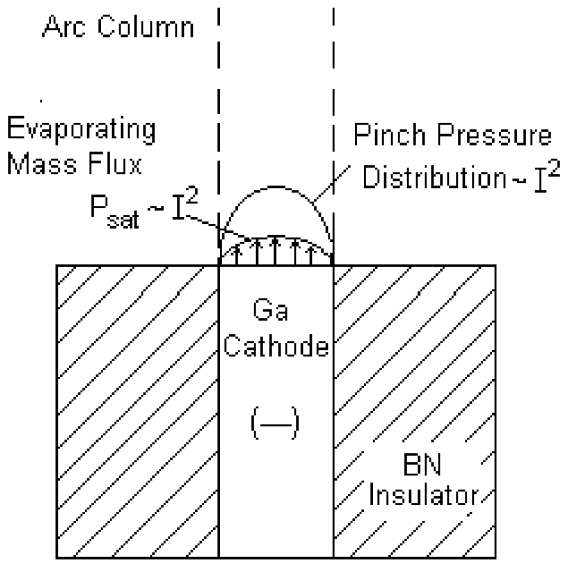

Figure 16. High current pinch discharge with evaporating gallium electrode.

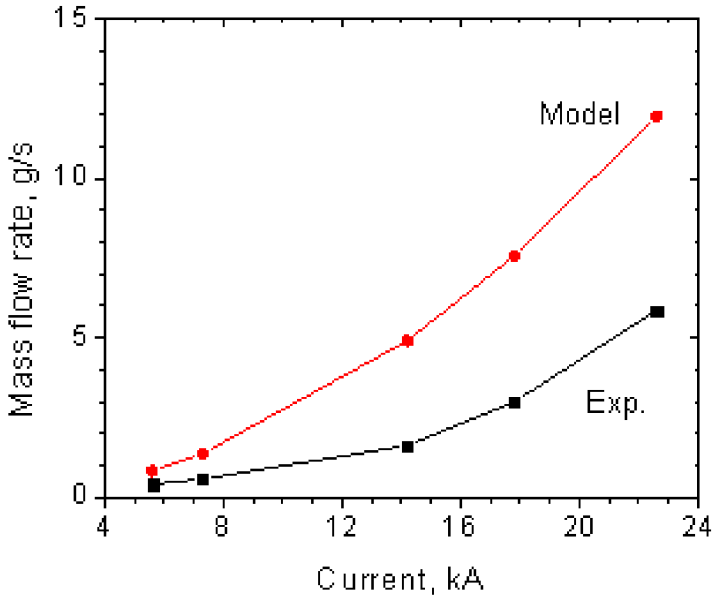

Figure 17. Experimental and calculated mass flow rates.

V. Summary

The results obtained can be summarized as follows:

- Experiments were conducted at discharge currents spanning a range from 7-23 kA utilizing a central gallium electrode. When using a central gallium anode, macroparticles were ejected at all energy levels tested. Macroparticles were ejected using the central gallium cathode when the current density exceeded 3.7 $\times 10^8$ A/m^2.

- The measured mass bit follows a quadratic dependence on the discharge current. This yields a constant exhaust velocity of 17 km/s and 20 km/s for radius ratios of 2.6 and 3.4, respectively, and a predicted velocity of 23 km/s for a radius ratio of 5.0.
- The performance increases as the radius ratio of the thruster increases. An efficiency of 30% was obtained with a radius ratio of 3.4, and would be raised to 40% for a radius ratio of 5.0
- Triple Langmuir probe measurements along the center-line of the thruster yield a peak electron temperature and density of 3.8 eV and 1.6 $^{21}m^{-3}$ two centimeters from the cathode tip. The axial measurements suggest a well collimated exhaust plume with a divergence angle of 9°, and fully doubled ionized plasma at the cathode surface.
- Emission spectroscopy was used to determine the species present in the discharge as a function of discharge current. Ga I-III lines were present at all energy levels. The number of doubly ionized gallium and iron (from the outer electrode) lines increased as the current increased.

Appendix

Table 2. Neutral and ionic gallium species present in 22 kA arc discharge.

Specie	Wavelength, nm	Upper Energy Level, cm^{-1}	Lower Level	Upper Level
Ga I	223.592	45071.75	$3d^{10}4s^24p$	$4s^27d$
Ga I	229.786	44332.27	$3d^{10}4s^24p$	$4s^28s$
Ga I	233.824	43580.44	$3d^{10}4s^24p$	$4s^26d$
Ga I	245.007	40802.86	$3d^{10}4s^24p$	$4s^25d$
Ga I	260.734	38341.72	$3d^{10}4s^24p$	$4s4p^2$
Ga I	294.417	34787.85	$3d^{10}4s^24p$	$4s^24d$
Ga I	403.298	24.788.53	$3d^{10}4s^24p$	$4s^25s$
Ga I	417.204	24788.53	$3d^{10}4s^24p$	$4s^25s$
Ga II	231.727	113842.30	4s4p	4s4d
Ga II	235.532	156327.39	4s4d	4s7f
Ga II	251.403	147485.46	$4p^2$	4s5f
Ga II	277.997	106662.37	4s4p	4s5s
Ga II	299.265	151923.93	4s5p	4s8s
Ga II	337.595	137342.57	$4p^2$	4s4f
Ga II	347.208	147520.34	4s5p	4s6d
Ga II	425.593	137332.28	4s4d	4s4f
Ga III	208.948	209148.01	$3d^{10}5p$	$3d^{10}7s$
Ga III	236.866	227637.2	$3d^{10}4f$	$3d^{10}7g$
Ga III	241.787	185432.59	$3d^{10}4d$	$3d^{10}4f$
Ga III	242.454	185432.59	$3d^{10}4d$	$3d^{10}4f$
Ga III	351.737	189187.72	$3d^{10}5p$	$3d^{10}5d$
Ga III	438.184	208254.14	$3d^{10}4f$	$3d^{10}5g$
Ga III	486.303	161304.40	$3d^{10}5s$	$3d^{10}5p$
Ga III	499.393	160765.56	$3d^{10}5s$	$3d^{10}5p$

References

[1]Polzin, K., Markusic, T., Burton, R., Thomas, R., and Carroll, D., "Gallium Electromagnetic (GEM) Thruster Concept and Design," *42nd AIAA/ASME/SAE/ASEE Joint Propulsion Conference*, July 9-12 2006.

[2]Thomas, R., Burton, R., Glumac, N., and Polzin, K., "Preliminary Spectroscopic Measurements for a Gallium Electromagnetic (GEM) Thruster," *43rd AIAA/ASME/SAE/ASEE Joint Propulsion Conference*, July 8-11 2007.

[3]Thomas, R., Burton, R., and Polzin, K., "Preliminary Development and Testing of a Self-Injecting Gallium MPD Thruster," *44th AIAA/ASME/SAE/ASEE Joint Propulsion Conference & Exhibit*, 21 - 23 July 2008.

[4]Jahn, R., *Physics of Electric Propulsion*, McGraw-Hill, 1968.

[5]Laystrom, J. and Burton, R., "Geometric Optimization of a Coaxial Pulsed Plasma Thruster," *39th AIAA/ASME/SAE/ASEE Joint Propulsion Conference*, July 20-23 2003.

[6]Paccani, G., Chiarotti, U., and Deininger, W. D., "Quasi-steady Ablative Magnetoplasmadynamic Thruster Performance with Different Propellants," *Journal of Propulsion and Power*, Vol. 14, No. 2, March-April 1998.

[7]Ducati, A. and Jahn, R., "Investigation of Pulsed Quasi-Steady MPD Arc Jets," Tech. Rep. FR-061-10140, Plasmadyne, 1971.

[8]Chen, S.-L. and Sekiguchi, T., "Instantaneous Direct-Display System of Plasma Parameters by Means of Triple Probe," *Journal of Applied Physics*, Vol. 36, No. 8, August 1965.

[9]Burton, R., DelMedico, S., and Andrews, J., "Application of a Quadruple Probe Technique to MPD Thruster Plume Measurements," *Journal of Propulsion and Power*, Vol. 9, No. 5, 1993.

[10]Gallimore, A., Kelly, A., and Jahn, R., "Anode Power Deposition in Magnetoplasmadynamic Thrusters," *Journal of Propulsion and Power*, Vol. 9, No. 3, 1993.

[11]Tilley, D., Kelly, A., and Jahn, R., "The Application of the Triple Probe Method to MPD Thruster Plumes," *21st International Electric Propulsion Conference*, July 18-20 1990.

[12]Peterson, E. and Talbot, L., "Collisionless Electrostatic Single-Probe and Doube-Probe Measurements," *AIAA Journal*, Vol. 8, No. 12, 1970, pp. 2215–2219.

[13]Boxman, R. L., Sanders, D. M., and Martin, P. J., editors, *Handbook of vacuum arc science and technology : fundamentals and applications*, Noyes Publications, 1995.

[14]Geiger, F., Busse, C., and Loehrke, R., "The Vapor Pressure of Indium, Silver, Gallium, Copper, Tin, and Gold Between 0.1 and 3.0 Bar," *International Journal of Thermophysics*, Vol. 8, No. 4, 1987.